Earth and Planetary Science Letters 453 (2016) 171–181

Contents lists available at ScienceDirect

Earth and Planetary Science Letters

www.elsevier.com/locate/epsl

The effects of magmatic processes and crustal recycling on the molybdenum stable isotopic composition of Mid-Ocean Ridge Basalts

Rachel Bezard [a,*], Mario Fischer-Gödde [a], Cédric Hamelin [b], Gregory A. Brennecka [a], Thorsten Kleine [a]

[a] Institut für Planetologie, University of Münster, Wilhelm-Klemm-Str. 10, 48149 Münster, Germany
[b] Department of Earth Science, University of Bergen, Norway

ARTICLE INFO

Article history:
Received 29 February 2016
Received in revised form 28 July 2016
Accepted 29 July 2016
Available online 25 August 2016
Editor: B. Marty

Keywords:
molybdenum stable isotopes
MORBs
mantle
partial melting
crustal recycling

ABSTRACT

Molybdenum (Mo) stable isotopes hold great potential to investigate the processes involved in planetary formation and differentiation. However their use is currently hampered by the lack of understanding of the dominant controls driving mass-dependent fractionations at high temperature. Here we investigate the role of magmatic processes and mantle source heterogeneities on the Mo isotope composition of Mid-Ocean Ridges Basalts (MORBs) using samples from two contrasting ridge segments: (1) the extremely fast spreading Pacific–Antarctic (66–41°S) section devoid of plume influence and; (2) the slow spreading Mohns–Knipovich segment (77–71°N) intercepted by the Jan Mayen Plume (71°N). We show that significant variations in Mo stable isotope composition exist in MORBs with $\delta^{98/95}$Mo ranging from −0.24‰ to +0.15‰ (relative to NIST SRM3134). The absence of correlation between $\delta^{98/95}$Mo and indices of magma differentiation or partial melting suggests a negligible impact of these processes on the isotopic variations observed. On the other hand, the $\delta^{98/95}$Mo variations seem to be associated with changes in radiogenic isotope signatures and rare earth element ratios (e.g., $(La/Sm)_N$), suggesting mantle source heterogeneities as a dominant factor for the $\delta^{98/95}$Mo variations amongst MORBs. The heaviest Mo isotope compositions correspond to the most enriched signatures, suggesting that recycled crustal components are isotopically heavy compared to the uncontaminated depleted mantle. The uncontaminated depleted mantle shows slightly sub-chondritic $\delta^{98/95}$Mo, which cannot be produced by core formation and, therefore, more likely result from extensive anterior partial melting of the mantle. Consequently, the primitive $\delta^{98/95}$Mo composition of the depleted mantle appears overprinted by the effects of both partial melting and crustal recycling.

1. Introduction

High-temperature stable isotope fractionations can provide important insights into the nature and conditions of the processes involved in planetary differentiation, such as core formation, crust production and crust–mantle interaction (e.g. Georg et al., 2007; Dauphas et al., 2009; Cabral et al., 2013). Based on experimental work showing that resolvable Mo isotopic fractionation exists between liquid silicate and liquid metal up to temperatures of ~2500 °C, Mo isotopes have much potential to investigate the conditions of core formation in the Earth and other planetary bodies (e.g., Hin et al., 2013; Burkhardt et al., 2014). However, the use of this experimental calibration to constrain core formation temperature requires the Mo isotopic composition of both the core and the silicate portion of the Earth to be precisely known. While a $\delta^{98/95}$Mo of -0.16 ± 0.02‰ (relative to NIST SRM3134) can be assumed for the core (Burkhardt et al., 2014), a precise estimate of the Mo stable isotope composition for the bulk silicate Earth (BSE) is more difficult to obtain. This is because the current BSE comprises several reservoirs for which the production and/or evolution likely involved Mo isotopic fractionation. Indeed, the Mo stable isotope compositions of terrestrial igneous rocks vary by more than 1‰ (Burkhardt et al., 2014; Freymuth et al., 2015; Greber et al., 2014, 2015; Neubert et al., 2011; Siebert et al., 2003; Voegelin et al., 2012, 2014; Yang et al., 2015). These large isotopic variations either result from isotopic fractionation during magma production and differentiation, or reflect isotopic heterogeneities in the mantle source created by crustal recycling. One approach to constrain the Mo isotopic composition of the BSE is to analyse komatiites. This is because these volcanic rocks were formed by large-scale melting at very high temperatures, limiting poten-

* Corresponding author. Fax: +49 251 83 36301.
E-mail address: bezard@wwu.de (R. Bezard).

http://dx.doi.org/10.1016/j.epsl.2016.07.056

tial isotopic fractionation during partial melting. Using komatiites, Greber et al. (2015) argued that the Mo stable isotope composition of the BSE is indistinguishable from the composition of the bulk Earth as estimated from chondrites and iron meteorites (Burkhardt et al., 2014). However, the komatiites themselves showed rather large variations in $\delta^{98/95}$Mo with a total spread of ~0.8‰ that was likely produced by crustal assimilation during magma ascent or post-emplacement isotopic fractionation (Greber et al., 2015). These variations, and the lack of a clear understanding of the processes controlling them, make the precise determination of the Mo stable isotopic composition of the BSE difficult. In the light of these complexities, and given the importance of precisely knowing the Mo stable isotope composition of the BSE for constraining core formation, it is important to further investigate this composition using another approach.

Another way to determine the Mo stable isotope composition of the BSE is to use recent oceanic basalts. The advantages of using recent oceanic basalts over komatiites include (1) the availability of fresh samples, limiting the chances of post-emplacement isotopic fractionation, as well as (2) a good knowledge of the conditions and geodynamical contexts of eruption and (3) the possibility to select representative samples covering the full range of mantle compositional variations defined by radiogenic isotopes and trace element concentrations. Nonetheless, whether the Mo stable isotope composition of oceanic basalts reflect those of their mantle sources, i.e., whether magmatic processes fractionate the mantle signature, remains to be further investigated. Indeed, Mo isotope fractionation during mantle partial melting has not yet been tested. Furthermore, isotopic fractionation during magma differentiation was not systematically observed. It was suggested to occur in hydrous arc rocks by Voegelin et al. (2014), based on correlations between Mo isotopes and indices of differentiation for a suite of igneous rocks from the Aegean arc (and heterogeneous $\delta^{98/95}$Mo in mineral separates), but was neither recorded in the case of Mariana Arc lavas (Freymuth et al., 2015) or in Iceland lavas from the Hekla volcano (Yang et al., 2015).

Up to now, only a limited Mo stable isotope data set exists for oceanic basalt and it remains unconstrained as to whether parts of the current mantle could have preserved the BSE composition. Overall, little is known about the impact of the main differentiation processes, i.e., partial melting and crustal recycling, on the mantle $\delta^{98/95}$Mo. Nevertheless, mantle heterogeneities related to crustal recycling are predicted based on arc studies (Freymuth et al., 2015; König et al., 2016). These investigations suggest that Mo stable isotopes fractionation in oceanic crust and sediments occurs during subduction, resulting in a lighter signature for the slab after dehydration. Thus, the incorporation of residual slabs to the mantle likely results in Mo isotope variations in the mantle. On the other hand, the Mo signature of arc rocks does not provide information about the impact of partial melting on the Mo isotope composition of the mantle because the Mo of arc lavas dominantly originates from the subducting slab, not the mantle wedge (Freymuth et al., 2015). In other words, partial melting alone may not produce Mo isotopic fractionation and mantle zones devoid of recycled oceanic crust may, therefore, have preserved their primitive composition.

Here we address the role of magmatic processes and mantle source heterogeneities on the Mo stable isotopic composition of Mid-Ocean Ridge Basalts (MORBs) using volcanic glasses from two contrasting ridges: Pacific–Antarctic (66–41°S) and Mohns–Knipovich (77–71°N) including a sample from the intercepting Jan Mayen plume (Elkins et al., 2016). In addition to providing the first extensive dataset for Mo stable isotopes in MORBs, our results provide critical information for the appraisal of the Mo stable isotope composition of the BSE.

2. Samples and analytical method

2.1. Samples

We selected twenty MORB glasses from the Pacific–Antarctic ridge (66–41°S; Fig. 1a) as well as seven glasses from the Mohns–Knipovich ridges (77–71°N) and one Oceanic Island Basalt (OIB) from Jan Mayen Island (71°N), which is located on the southern extremity of the Mohns ridge (Fig. 1b). The Pacific–Antarctic MORBs were sampled during the oceanographic cruises PACANTARCTIC (PAC1; 66–56°S) and PACANTARCTIC 2 (PAC2; 53–41°S). Amongst these samples, fourteen represent magmas erupted through the ridge axis while six were erupted off-axis. For all the on-axis glasses, major and trace elements (including Cl and S) as well as Sr, Nd, Pb, Hf and S isotope data are available (and He and Ne isotopes for some samples; Hamelin et al., 2010, 2011; Labidi et al., 2014; Moreira et al., 2008; Vlastélic et al., 1999, 2000). The off axis samples are characterised in terms of major elements, Cl and S concentrations and Pb and S isotopes. All on-axis Pacific–Antarctic samples are N-MORBs ('normal' MORBs, defined by $La/Sm_N < 1$) except for one sample displaying a T-MORB composition ('transitional' MORBs, defined by $1 < La/Sm_N < 1.7$). Based on their location and radiogenic isotope signatures, Pacific–Antarctic magmas were suggested to be devoid of mantle plume influence (e.g. Dosso et al., 2005). Mohns–Knipovich MORBs (77–71°N) and Jan Mayen (71°N) Oceanic Island Basalt (OIB) were sampled during the Norwegian sampling program, SUBMAR (four different cruises between 2000 and 2003 onboard the R.V. Håkon Mosby). Major and trace elements as well as Sr, Nd, Hf and Pb isotopic compositions are available for two of the seven samples selected (Elkins et al., 2016).

The Pacific–Antarctic samples are well suited to constrain how the Mo stable isotopic composition of magmas changes with the dominant magma differentiation processes occurring at mid-ocean ridges: mineral fractionation and crustal/hydrothermal fluid assimilation. Although the samples are not cogenetic, they evolved under similar magmatic conditions and cover the range of MgO typically observed at mid-ocean ridges (MgO = 4–10 wt.%). Diagrams in which various major elements are plotted versus MgO (wt.%) illustrate this common liquid line of descent for samples that are spread over 1000 km of a ridge section (supplementary figure in Hamelin et al., 2010). Furthermore, the selected samples have previously been shown to be variably affected by crustal and hydrothermal fluid assimilation (Labidi et al., 2014), allowing the impact of such processes on Mo isotopes to be constrained.

Pacific–Antarctic and Mohns–Knipovich MORBs together are pertinent to investigate the effect of mantle partial melting since they allow comparison between magmas typically formed by high, moderate and low degrees of partial melting occurring at fast (northern Pacific–Antarctic segment investigated; PAC2 samples; up to 110 mm/yr; DeMets et al., 1990), intermediate (southern Pacific–Antarctic segment; PAC1 ~55 mm/yr; DeMets et al., 1990) and slow ridge segments (Mohns–Knipovich; ~15 mm/yr; Dick et al., 2003), respectively. In addition, the comparison of the Mohns–Knipovich MORBs with the Jan Mayen OIB could provide further insights into the impact of partial melting on Mo isotopic compositions, given the very distinct degrees of melting for MORBs and OIBs.

Finally, the selected Pacific–Antarctic and Mohns–Knipovich samples are also relevant to explore the role of mantle heterogeneities. Based on radiogenic isotope compositions (e.g., Fig. 2), the source of Pacific–Antarctic MORBs comprises dominantly depleted Mantle (DMM) as well as small amounts of recycled oceanic crust, with both components thought to be intrinsic to the asthenospheric mantle (i.e., no plume from the deeper mantle involved; e.g. Hamelin et al., 2011). The source of Mohns–Knipovich

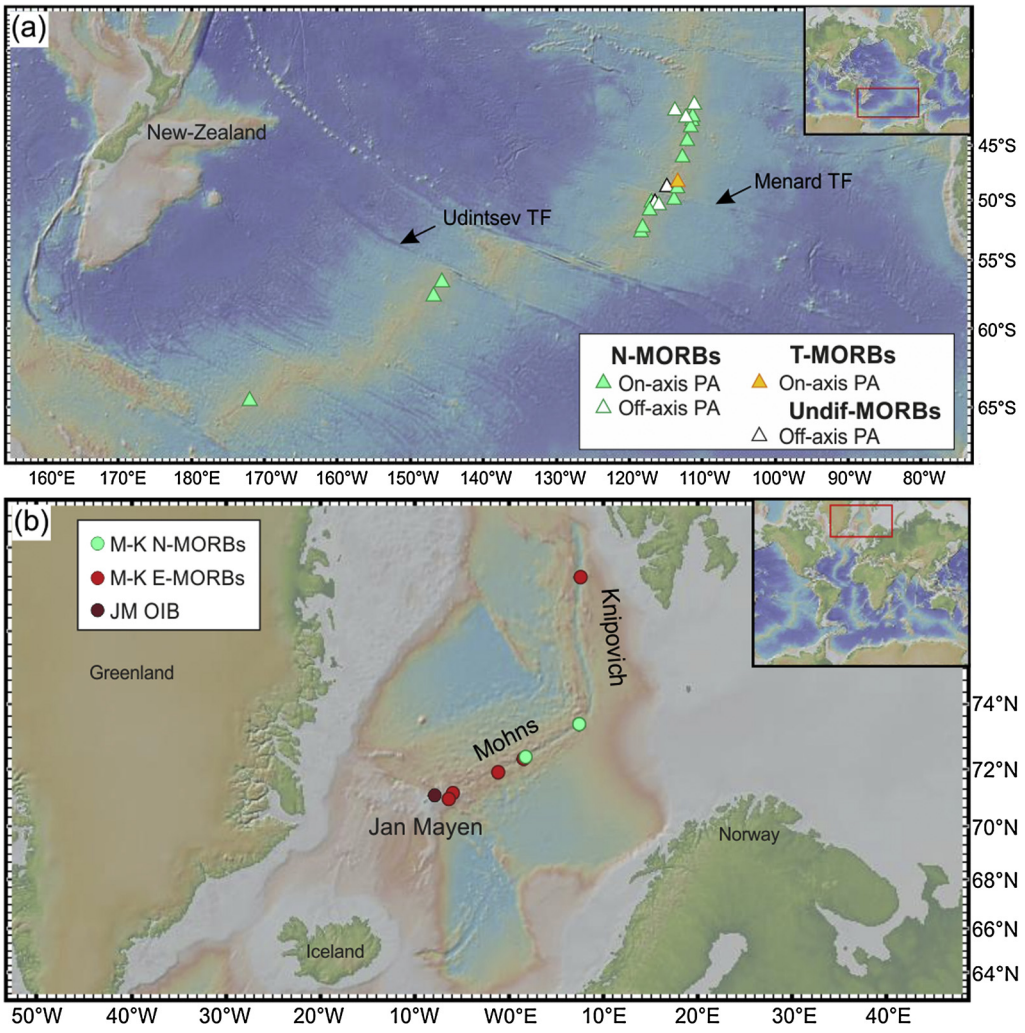

Fig. 1. Map of the two sample localities: (a) Pacific–Antarctic (PA) ridge segment between 30 and 68°S and (b) Mohns–Knipovich (M–K) ridges and Jan-Mayen (JM) ocean island. N- T- E- and Undif. MORBs: normal ($(La/Sm)_N < 1$), transitional ($1 < (La/Sm)_N < 1.7$), enriched ($(La/Sm)_N > 1.7$) and undifferentiated mid-ocean ridge basalts, respectively. OIB: oceanic island basalt. Major transform faults (TF) close to the sample locations are also shown.

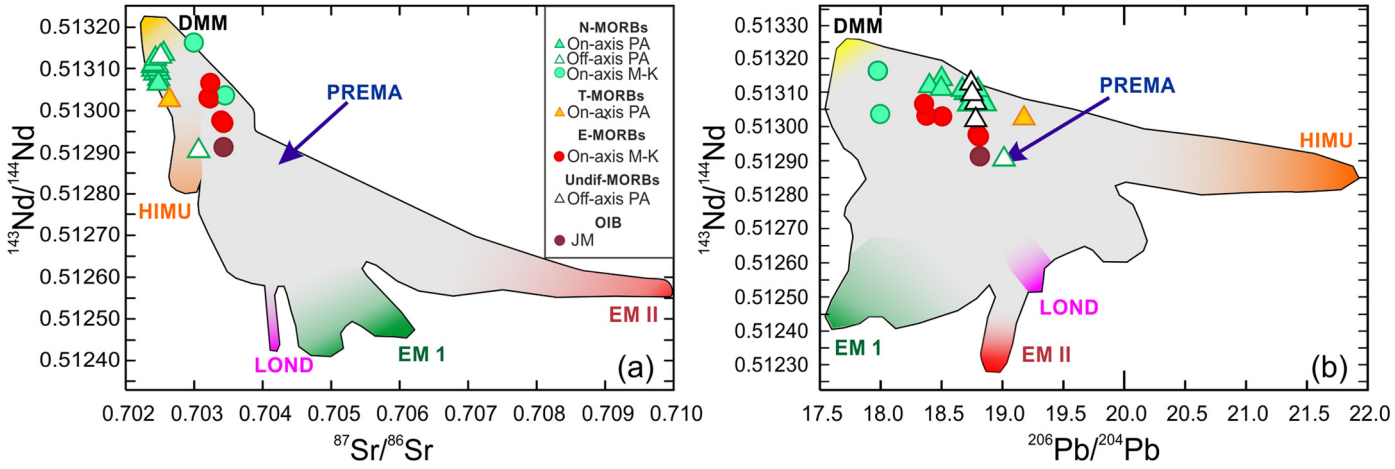

Fig. 2. Sr, Nd and Pb isotopic composition of all the on-axis Mid-ocean ridge basalts (MORBs) analysed, Jan-Mayen (JM) Oceanic-island basalt (OIB) and two representative off-axis MORBs. M–K: Mohns–Knipovich ridges; PA: Pacantactic ridge. N- T- E- and Undif. MORBs: normal, transitional enriched and undifferentiated mid-ocean ridge basalts respectively (as defined in Fig. 1 caption). DMM = depleted MORB mantle; HIMU = mantle source characterised by high μ values ($\mu = (^{238}U/^{204}Pb)_{t=0}$); PREMA = prevalent mantle; EM I & 2 = enriched mantle-1 and 2, respectively; LOND = endmember with low εNd for a given $^{87}Sr/^{86}Sr$ compared to EM I (see White, 2015). Data sources: Sr, Nd, Hf and Pb isotopes of on-axis PA ridge basalts: Vlastélic et al. (1999) and Vlastélic et al. (2000); Moreira et al. (2008); Hamelin et al. (2010, 2011); Sr, Nd, Hf and Pb isotopes of PA off-axis, M–K MORBs and JM OIB: Elkins et al. (2016) and this study. Field: global oceanic basalt composition as presented in White (2015) with data from the EarthChemdatabases (www.earthchem.org). Position of DMM, HIMU, PREMA, LOND, EM I and EM II endmembers are from White (2015).

MORB comprises two other main components: (1) a peculiar depleted endmember (characterised by Hf isotopic composition that is too radiogenic to plot on the typical MORB-OIB trend) suggested to be dominated by sub-continental lithospheric mantle and (2) variable amounts of the Jan Mayen plume material characterised by an intermediate Sr, Nd, Pb and Hf isotopic compositions amongst oceanic basalts (Blichert-Toft et al., 2005; e.g. Fig. 2). Thus, by using Pacific–Antarctic, Mohns–Knipovich and Jan Mayen samples together, the impact of source heterogeneity on Mo stable isotopes can be investigated.

2.2. Analytical method

The Mo stable isotope compositions and Mo concentrations were analysed for all samples using double spike MC-ICPMS. Major and trace elements as well as various radiogenic and stable isotope compositions were already available for many of the samples selected (as detailed in the previous section) and were obtained for some samples as explained in the Supplementary Material.

For all samples analysed, glass was crushed into 1 mm fragments and hand-picked to select the freshest and mineral-free material. The fragments were subsequently powdered using an agate mortar. For each sample, between 50 and 300 mg of glass powder was weighted in 15 ml Savillex beakers and spiked with a mixed ^{97}Mo–^{100}Mo tracer in order to correct for possible mass fractionation occurring during chemistry and mass-spectrometry [see Hin et al. (2013) and Burkhardt et al. (2014) for information on the preparation and calibration of the ^{97}Mo–^{100}Mo double spike]. The spiked powders were digested in HF-HNO_3 with traces of $HClO_4$ for 72 h on the hotplate at 180 °C. After drying, the samples were re-dissolved and dried again in conc. HNO_3 and conc. HCl. Molybdenum was separated from the sample matrix by a three stage column chemistry, using cation (BioRad AG50W-X8), anion (AG1X8) and TRU-Spec resin (Burkhardt et al., 2014).

The Mo isotope measurements were conducted using the ThermoScientific Neptune*Plus* MC-ICPMS in the Institut fur Planetologie at the University of Münster. Samples were dissolved in 0.5M HNO_3–0.05M HF and introduced into the mass spectrometer using a Cetac Aridus II desolvator and an ESI Microflow PFA nebulizer with an uptake rate of ∼60 µl/min.

Using this setup in combination with Ni H-cones yielded a sensitivity of ∼155 V/ppm. Samples were typically analysed at 50–70 ng/g, for which total ion beam intensities between $\sim 8 \times 10^{-11}$ and $\sim 1.1 \times 10^{-10}$ A were obtained.

The Mo stable isotope measurements were done in static mode and ^{95}Mo, ^{97}Mo, ^{98}Mo and ^{100}Mo, (i.e., the isotopes used in the double spike deconvolution) as well as ^{99}Ru were monitored simultaneously using Faraday cups. All cups were connected to amplifiers with 10^{11} Ω feedback resistors, except the cup used for ^{99}Ru for which a 10^{12} Ω resistor was employed. Each analysis consisted of an on-peak baseline measurement on a blank solution (0.5M HNO_3–0.05M HF) of 10 integrations of 4 s followed by 80 integrations of 4 s of sample or standard solution.

The data deconvolution as well as the correction for isobaric Ru interferences were done off-line using the 'double spike toolbox' (Rudge et al., 2009), in which we implemented a script that iteratively corrects for Ru interference. The double spike inversion yields both the Mo isotopic composition and concentration of the sample.

Each sample analysis was bracketed by measurements of a spiked NIST SRM3134 standard solution (Greber et al., 2012; Goldberg et al., 2013) and the results are reported in $\delta^{98/95}$Mo notation expressed as

$$\delta^{98/95}\mathrm{Mo} = -1000\left(\alpha_{\mathrm{sample}} - \alpha^{\mathrm{mean}}{}_{\mathrm{SRM3134}}\right)\ln(m_{98}/m_{95})$$

representing the ‰ deviation of the alpha of a sample (α_{sample}) from the mean alpha of the two bracketing SRM3134 standards ($\alpha^{m}{}_{\mathrm{SRM}}$); m_{98} and m_{95} correspond to the atomic weights of ^{98}Mo and ^{95}Mo. Ru interference corrections were always applied and were typically < 0.01‰ and never exceeded 0.05‰.

Replicate digestions of USGS geological reference materials W-2a ($n = 6$) and BHVO-2 ($n = 6$) yielded isotope compositions of -0.04 ± 0.03‰ (2 s.d.) and -0.08 ± 0.06‰, respectively (see Supplementary Material). These values are identical within uncertainties to the values of Burkhardt et al. (2014) (W-2a = -0.05 ± 0.06‰; BHVO-2 = -0.06 ± 0.03‰), Freymuth et al. (2015) (BHVO-2 = -0.08 ± 0.08‰), Willbold et al. (2016) (BHVO-2 = -0.07 ± 0.04‰) and Yang et al. (2015) (BHVO-2 = $+0.01 \pm 0.06$‰). The MORB samples investigated in the present study were analysed between 1 and 8 times and a single digestion was never analysed more than twice. For samples analysed less than four times, uncertainties correspond to twice the standard deviation obtained for replicate analyses of the USGS standards (±0.05‰); for samples analysed four times or more 95% confidence intervals are given. The Mo concentrations for W-2 and BHVO-2 obtained from the deconvolution were 0.400 ± 0.009 µg/g (2 s.d., $n = 6$) and 3.8 ± 1.8 µg/g (2 s.d., $n = 6$). Both values are in good agreement with Burkhardt et al. (2014) (W-2a = 0.393 ± 0.004 µg/g and BHVO-2 ∼4.55 µg/g), Freymuth et al. (2015) (BHVO-2 = 3.4 ± 2.5 µg/g), Yang et al. (2015) (BHVO-2 = 3.5 ± 0.9 µg/g) and Willbold et al. (2016) (BHVO-2 = 4.2 ± 1.8 µg/g). The high variability of BHVO-2 has been noted by all previous authors and probably results from heterogeneous contamination of the powder during its preparation (e.g. Weis et al., 2005; Willbold et al., 2016).

3. Results

All $\delta^{98/95}$Mo and Mo concentration data are presented in Table 1. The corresponding new MgO, $(La/Sm)_N$ and Sr, Nd, Hf and Pb isotope data are presented in Table 2 together with the literature data. The complete set of new and published major and trace element concentrations and isotopic data are shown in the Supplementary Material.

3.1. $\delta^{98/95}$Mo and Mo concentrations

The $\delta^{98/95}$Mo values of the investigated MORBs range from −0.24‰ to 0.15‰ and the Jan Mayen OIB signature ($\delta^{98/95}$Mo = −0.10‰) overlaps the MORBs spectrum (Fig. 3). Pacific–Antarctic on-axis glasses exhibit lighter-than-chondritic to chondritic compositions ($\delta^{98/95}$Mo = −0.22 to −0.13‰ ($n = 13$); Chondrites $\delta^{98/95}$Mo = -0.16 ± 0.02‰; Burkhardt et al., 2014) except for one sample erupted at the Menard transform fault (TF; a first order ridge discontinuity thought to separate two slightly different mantle domains; Hamelin et al., 2010). This sample (PAC2DR22-1) displays a heavy Mo isotope composition with $\delta^{98/95}$Mo = +0.13‰ (Fig. 4). The Pacific–Antarctic off-axis samples show greater Mo isotope variability ($\delta^{98/95}$Mo = −0.24 to 0.15‰) compared to the on-axis samples. All the off-axis samples with heavier-than-chondritic $\delta^{98/95}$Mo were erupted in the vicinity of the Menard TF (Fig. 4), while the three remaining off-axis samples, with sub-chondritic $\delta^{98/95}$Mo, were erupted further North on small volcanic ridges (40–42°N). The Mohns–Knipovich and Jan Mayen samples have $\delta^{98/95}$Mo overlapping the heaviest Pacific–Antarctic on-axis glass compositions but also display heavier $\delta^{98/95}$Mo values ranging from −0.08 to 0.15‰ (Fig. 3).

Molybdenum concentrations range from 231 to 1185 ng/g in the on-axis Pacific–Antarctic glasses and from 93 to 503 ng/g in the off-axis samples (Fig. 5a). The Mohns–Knipovich samples (147 to 1882 ng/g Mo) show a much larger range in Mo concentrations

Table 1
$\delta^{98/95}$Mo and Mo concentration of the Pacific Antarctic, Mohns–Knipovich and Jan Mayen samples. Sample type and location are also listed.

Sample	Sample type	Position	Latitude	Longitude	N[a]	$\delta^{98/95}$Mo (‰)	Error[b]	Mo (ng/g)[c]
Pacific–Antarctic ridge								
PAC1CV03g	N-MORB	On-axis	−64.53	171.88	2 (2)	−0.22	0.05	184
PAC1DR11-1	N-MORB	On-axis	−57.63	146.80	4 (2)	−0.20	0.06	185
PAC1DR13-2	N-MORB	On-axis	−56.57	145.74	4 (2)	−0.18	0.06	263
PAC2DR01-1	N-MORB	On-axis	−52.53	118.35	2 (1)	−0.17	0.05	323
PAC2DR02-1	N-MORB	On-axis	−52.13	118.13	8 (4)	−0.18	0.03	389
PAC2DR06-6	N-MORB	On-axis	−50.70	117.19	4 (2)	−0.19	0.05	1026
PAC2DR16-1g (a)	N-MORB	Off-axis	−50.20	115.89	6 (3)	0.14	0.02	514
PAC2DR16-1g (b)					2 (1)	0.16	0.05	493
PAC2DR11-3g	–	Off-axis	−50.07	116.47	3 (2)	−0.12	0.05	257
PAC2DR08-1	N-MORB	On-axis	−49.99	116.97	3 (2)	−0.16	0.05	344
PAC2DR20-1	N-MORB	On-axis	−49.73	113.78	6 (3)	−0.15	0.02	804
PAC2DR22-1	N-MORB	On-axis	−48.73	113.37	4 (2)	0.13	0.06	456
PAC2DR25-1g	–	Off-axis	−48.61	114.79	1	−0.06	0.05	266
PAC2DR27-1g	T-MORB	On-axis	−48.18	113.34	4 (2)	−0.13	0.05	1185
PAC2DR31-3	N-MORB	On-axis	−45.85	112.69	5 (3)	−0.19	0.06	280
PAC2DR36-1g	N-MORB	On-axis	−42.95	111.56	4 (2)	−0.19	0.02	387
PAC2DR37-2	N-MORB	On-axis	−42.27	111.34	1	−0.16	0.05	354
PAC2DR42-1c	–	Off-axis	−41.93	112.16	2 (2)	−0.24	0.05	93
PAC2DR38-1	N-MORB	On-axis	−41.80	111.27	5 (3)	−0.18	0.06	231
PAC2DR39-4	N-MORB	Off-axis	−41.25	113.69	8 (4)	−0.22	0.04	201
PAC2DR43-1g	–	Off-axis	−40.54	111.03	2 (2)	−0.21	0.05	111
Mohns–Knipovich ridges								
SM02 DR014-03	E-MORB	On-axis	77.32	7.53	4 (2)	−0.10	0.03	1066
SM03 DR004-04	N-MORB	On-axis	73.41	7.41	6 (3)	−0.13	0.04	211
SM00 DR025-xx	N-MORB	On-axis	72.39	1.72	4 (2)	−0.15	0.03	147
SM00 DR002-36	E-MORB	On-axis	72.33	1.49	2 (1)	−0.08	0.05	908
SM03 DR052-1	E-MORB	On-axis	71.89	−1.19	2 (1)	−0.15	0.05	565
SM01 DR85-03	E-MORB	On-axis	71.20	−5.98	4 (2)	−0.12	0.04	1882
SM01 DR100-01	E-MORB	On-axis	70.99	−6.40	1	−0.11	0.03	1324
Jan Mayen island								
SM01 DR05-05	OIB	–	71.12	7.92	4 (2)	−0.10	0.03	2944

[a] N = number of analysis. The bracketed number corresponds the number of digestions.
[b] Error = mean 2 standard deviation of Geological reference materials for $N \leq 3$ and 95% Student-t distribution for $N > 3$.
[c] Uncertainty is ±2%, as defined by the 2 standard deviation of repeated W-2a digestion.

compared to the Pacific–Antarctic samples. Finally, the Jan Mayen OIB glass has 2944 ng/g Mo, the highest value obtained amongst the investigated samples.

3.2. Major and trace elements and radiogenic isotopes

The Nd isotope ratios obtained for the Pacific–Antarctic off-axis samples overlap on-axis compositions but also show some more radiogenic signatures with $^{143}Nd/^{144}Nd$ ranging between 0.512904 and 0.513131 (Fig. 6a). The greater compositional variability shown by the off-axis compared to the on-axis samples was also observed in other localities from the Pacific-ridge (e.g. Brandl et al., 2012). It was suggested to reflect upper mantle heterogeneities not otherwise observed in the on-axis ridges due to the 'compositional averaging' occurring during magma mixing in the main plumbing system (Rubin et al., 2009).

Mohns–Knipovich and Jan Mayen samples are basaltic with MgO between 4.8 and 8.7 wt.% (Table 2). Mohns–Knipovich samples consist of two and five sub-alkaline N- and E-MORBs, respectively. The Jan Mayen OIB sample has an alkaline composition. Trace element concentrations and radiogenic isotope compositions of the Mohns–Knipovich and Jan Mayen samples show the same range of composition as found by Blichert-Toft et al. (2005) at the same localities. N-MORBs have overlapping Sr and Nd isotopic compositions but more radiogenic Hf and less radiogenic Pb isotopic signatures compared to E-MORBs. The Jan Mayen OIB sample shows overlapping Sr isotope but less radiogenic Nd, Hf and more radiogenic Pb isotope compositions than E-MORBs (Table 2).

4. Discussion

4.1. Role of magma differentiation

Little is known about the impact of magma differentiation on Mo stable isotope compositions. Yet, understanding whether the Mo isotope composition measured for any MORB sample represents that of its respective primitive magma is critical to place any interpretation on mantle source compositions. In this section we discuss the impact of dominant processes involved during MORB differentiation-mineral fractionation and hydrothermal fluid or crust assimilation-on the Mo stable isotope composition of MORBs.

Pacific–Antarctic glasses present a wide range in MgO (4.4–9.5 wt.‰), and although not cogenetic, Pacific–Antarctic on-axis samples all share similar liquid lines of descent reflected by their common major and trace element differentiation trends (e.g., Mo in Fig. 5a; Al_2O_3, TiO_2, CaO, FeOt/MgO, $Na_2O + K_2O$ and S in the supplementary figures). The increase of Mo with decreasing MgO shown in Fig. 5a suggests that mineral fractionation dominantly controls Mo concentrations, which makes the Pacific–Antarctic suite suitable to investigate the impact of magma differentiation on Mo isotopes. This is for example not the case for the Mohns–Knipovich samples, where Mo concentrations correlate with indices of source enrichment (e.g. $^{143}Nd/^{144}Nd$; Fig. 7) suggesting that the Mo concentrations are controlled by the amount of Jan Mayen plume contribution (like other OIBs, Jan Mayen plume melts are enriched in incompatible elements). The strong incompatibility of Mo in Pacific–Antarctic on-axis samples, illustrated by its steep negative correlation with MgO, suggests limited fraction-

Table 2
MgO, $(La/Sm)_N$ and Sr, Nd Hf and Pb isotope compositions of the samples investigated. Previously published data are in italic font (Elkins et al., 2016; Hamelin et al., 2010; Moreira et al., 2008; Vlastélic et al., 1999, 2000).

Sample	MgO (wt.%)[a]	$(La/Sm)_N$	$^{87}Sr/^{86}Sr$	$^{143}Nd/^{144}Nd$	$^{176}Hf/^{177}Hf$	$^{206}Pb/^{204}Pb$	$^{207}Pb/^{204}Pb$	$^{208}Pb/^{204}Pb$
Pacific–Antarctic ridge								
PAC1CV03g	*8.63*	*0.66*	*0.702406*	*0.513117*	–	*18.497*	*15.498*	*38.093*
PAC1DR11-1	*7.58*	*0.58*	*0.702435*	*0.513125*	–	*18.401*	*15.494*	*37.862*
PAC1DR13-2	*7.50*	*0.62*	*0.702556*	*0.513142*	–	*18.500*	*15.497*	*37.966*
PAC2DR01-1	*7.40*	*0.81*	*0.702422*	*0.513090*	*0.28313*	*18.822*	*15.547*	*38.199*
PAC2DR02-1	*6.49*	*0.74*	*0.702417*	*0.513116*	*0.28314*	*18.724*	*15.530*	*38.110*
PAC2DR06-6	*4.41*	*0.89*	*0.702396*	*0.513099*	*0.28314*	*18.696*	*15.537*	*38.123*
PAC2DR16-1g	*8.16*	0.74	0.703065	0.512904	–	19.013	15.638	38.223
PAC2DR11-3g	*7.90*	–	–	0.513096	–	*18.746*	–	–
PAC2DR08-1	*7.12*	*0.93*	*0.702483*	*0.513077*	*0.28313*	*18.796*	*15.550*	*38.237*
PAC2DR20-1	*4.67*	*0.83*	*0.702493*	*0.513092*	*0.28313*	*18.749*	*15.540*	*38.168*
PAC2DR22-1	*7.32*	*0.70*	*0.702465*	*0.513100*	*0.28313*	*18.726*	*15.539*	*38.153*
PAC2DR25-1g	*8.01*	–	–	0.513019	–	*18.777*	–	–
PAC2DR27-1g	*4.62*	*1.23*	*0.702643*	*0.513035*	*0.28309*	*19.174*	*15.585*	*38.634*
PAC2DR31-3	*7.64*	*0.63*	*0.702479*	*0.513066*	*0.28311*	*18.858*	*15.580*	*38.300*
PAC2DR36-1g	*7.15*	*0.67*	*0.702479*	*0.513066*	*0.28312*	*18.724*	*15.538*	*38.117*
PAC2DR37-2	*7.84*	*0.65*	–	–	*0.28312*	–	–	–
PAC2DR42-1c	*9.50*	–	–	0.513070	–	*18.783*	–	–
PAC2DR38-1	*8.55*	*0.61*	*0.702465*	*0.513108*	*0.28313*	*18.671*	*15.533*	*38.039*
PAC2DR39-4	*8.88*	0.44	0.702514	0.513131	–	–	15.647	38.713
PAC2DR43-1G	*9.07*	–	–	0.513127	–	*18.741*	–	–
Mohns–Knipovich ridges								
SM02 DR014-03	7.46	2.21	0.703235	0.513068	0.28330	18.357	15.479	38.070
SM03 DR004-04	8.65	0.81	0.702995	0.513165	0.28341	17.977	15.422	37.646
SM00 DR025-xx	8.33	0.81	0.703451	0.513038	0.28338	17.996	15.423	37.689
SM00 DR002-36	7.30	2.86	0.703231	0.513031	0.28333	18.505	15.473	38.250
SM03 DR052-1	7.43	1.77	0.703210	0.513033	0.28332	18.376	15.452	38.101
SM01 DR85-03	7.26	3.86	0.703427	0.512972	0.28317	18.808	15.502	38.519
SM01 DR100-01	*6.10*	–	*0.703395*	*0.512978*	*0.28323*	*18.795*	*15.498*	*38.508*
Jan Mayen island								
SM01 DR05-05	*4.85*	*3.91*	*0.703430*	*0.512914*	*0.28309*	*18.815*	*15.506*	*38.587*

[a] Concentrations normalised to 100% volatile free.

ation of phases enriched in Mo. This includes MoS_2 (molybdenite), a phase shown to fractionate Mo isotopes significantly in magmas (Voegelin et al., 2012). Limited MoS_2 fractionation is also consistent with the incompatibility of S in the same set of samples (Labidi et al., 2014). The Mo incompatibility also suggests that, even if the fractionating assemblage preferentially incorporated lighter/heavier isotopes, the impact on the magma $\delta^{98/95}$Mo should be limited. This is confirmed in Fig. 5b, c which shows that $\delta^{98/95}$Mo does not vary systematically with the degree of differentiation, with the most evolved glass compositions overlapping within error those of the most mafic samples. This suggests that mineral fractionation cannot explain $\delta^{98/95}$Mo variations among the glasses.

Based on the systematics of the on-axis samples, isotopic variations observed in off-axis basalts are unlikely to be related to mineral fractionation if they fractionated the same phases. However, off-axis basalts were shown to each derive from primitive magmas with distinct compositions (major and trace element concentrations as well as radiogenic isotopes; see supplement) and oxygen fugacity compared to on-axis magmas. Furthermore, they differentiated in different plumbing systems (Brandl et al., 2012). Therefore, off-axis magmas could have fractionated different phases than the on-axis ones. Yet, all but one off-axis sample (PAC2DR16-1) plot on the on-axis Mo and S differentiation trend (Mo trend in Fig. 5a; S trend in the Supplementary Material). This suggests that their primitive magmas had a similar Mo concentration and that, if they fractionated a different assemblage, the difference could not be significant since it resulted in similar bulk Mo partition coefficients to that of the on-axis magmas (as expressed by the same slope for both on- and off-axis trends in the Mo versus MgO diagram). Furthermore, their very mafic nature (MgO > 7.9 wt.%) precludes an important volume of mineral fractionation. It is therefore unlikely that the variations observed for these off-axis samples result from mineral fractionation. The only off-axis sample (PAC2DR16-1) that does not plot on the Mo differentiation trend has a higher Mo concentration than other samples with similar MgO and also displays the heaviest isotopic signature ($\delta^{98/95}$Mo = $+0.15 \pm 0.02$‰). Such chemical and isotopic characteristics can, however, not be reconciled with mineral fractionation nor with accidental occurrence of mineral fragments in the crushed glass. Indeed, the magma is very mafic (MgO = 8.2 wt.%) precluding its higher Mo concentration to result from a greater amount of crystallisation of silicate phases. Fractionation of more Mo bearing accessory phases would all result in lower, instead of higher, Mo concentrations compared to the rest of the Pacific–Antarctic samples. The accidental presence of isotopically heavier phases in the glass picked is unlikely since the sample was analysed several times on two different powders made from different glass fragments (Table 1). Therefore, another process needs to explain the Mo concentration and heavy signature of this particular sample.

In summary, there is no noticeable impact of mineral fractionation on the Mo stable isotope composition of Pacific–Antarctic magmas. This is consistent with similar findings for samples from the Hekla volcano in Iceland (Yang et al., 2015), suggesting that, at least in dry magmas, mineral fractionation is not responsible for the $\delta^{98/95}$Mo variations observed among igneous rocks.

4.2. Role of crust and hydrothermal fluid assimilation

Other dominant processes occurring at Mid-oceanic Ridges are the interaction of magma with hydrothermally modified crust and

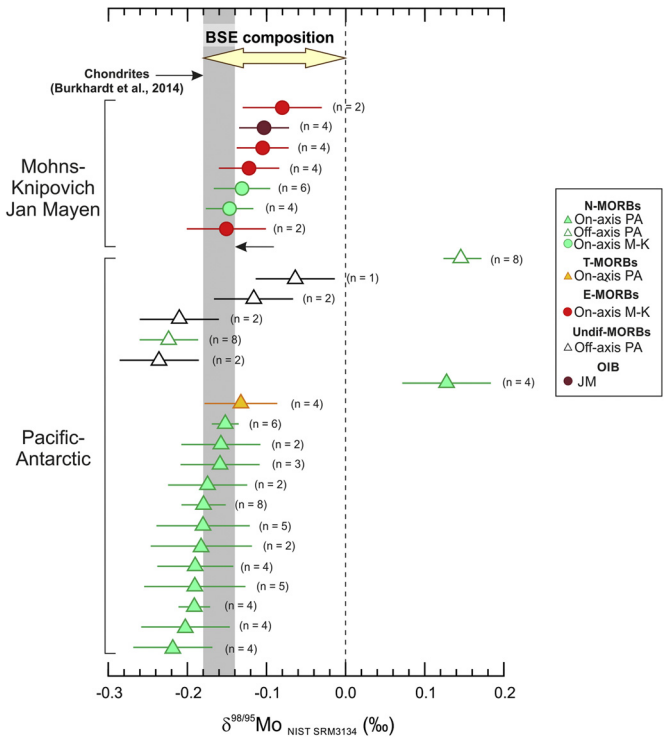

Fig. 3. $\delta^{98/95}$Mo of the oceanic basalts analysed. Abbreviations as in Fig. 2. Error = mean 2 s.d. of USGS standards (±0.05‰; $n \leq 3$) or 95% Student-t distribution ($n > 3$). Data are compared to the chondritic field of Burkhardt et al. (2014) since, based on experimental work from Hin et al. (2013), it represents the lowest $\delta^{98/95}$Mo possible for the Bulk Silicate Earth (BSE). The double-headed yellow arrow shows the most likely compositions for the BSE (Burkhardt et al., 2014), based on the experiments from Hin et al. (2013) and realistic core formation temperature for the Earth (≥1400 °C). (For interpretation of the references to colour in this figure legend, the reader is referred to the web version of this article.)

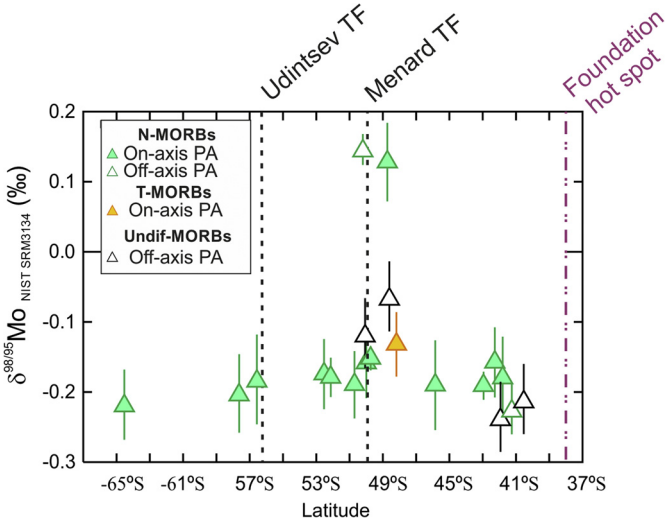

Fig. 4. Variation of $\delta^{98/95}$Mo with latitude amongst the Pacific–Antarctic ridge samples. Abbreviations as in Fig. 2. Udintsev and Menard transform faults (TF) as well as the Foundation hot spot locations are also shown.

with hydrothermal brines during its storage and ascent. These two processes were previously shown to affect magma compositions (e.g., Labidi et al., 2014) and could be responsible for some of the $\delta^{98/95}$Mo variations observed among MORBs. The impact of these processes can be assessed by exploring any $\delta^{98/95}$Mo correlation with key tracers already available for the Pacific–Antarctic samples (Labidi et al., 2014): Cl/K and δ^{34}S. Magma

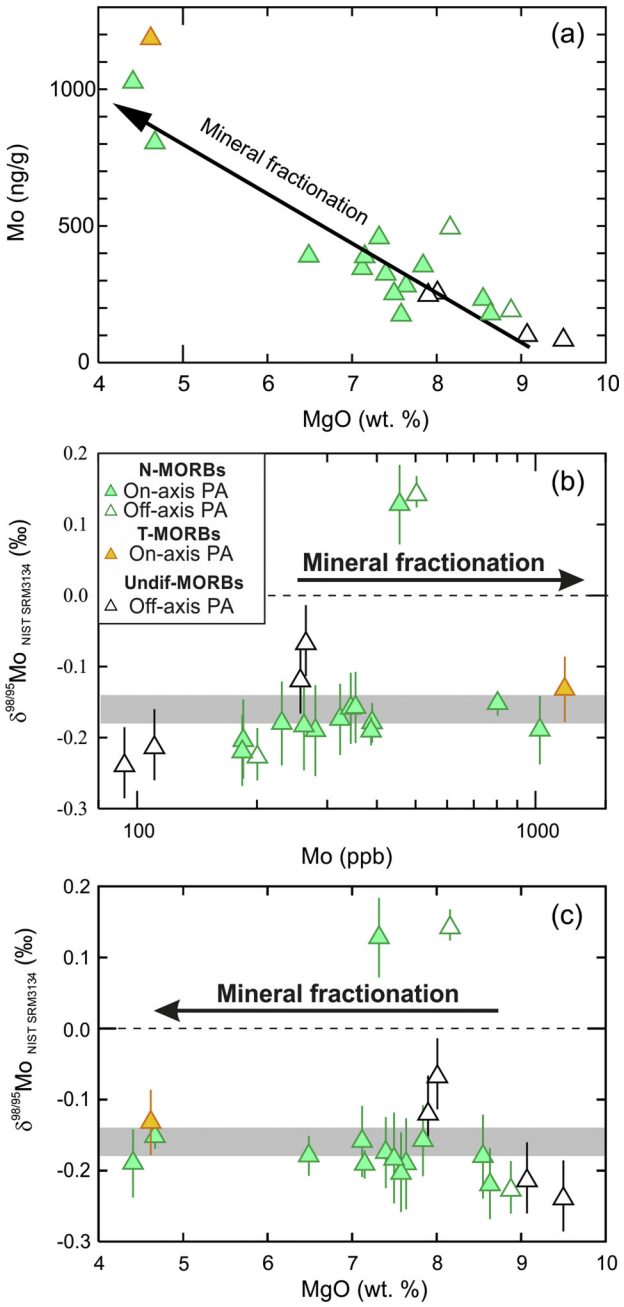

Fig. 5. (a) Mo (ng/g) vs. MgO. (b), (c) $\delta^{98/95}$Mo vs. Mo (ng/g) and MgO (wt.%). Abbreviations as in Fig. 2. In (b) and (c) Grey field: chondrite compositions of Burkhardt et al. (2014).

Cl/K increases with its interaction with hydrothermal brines (e.g. Michael and Cornell, 1998) while δ^{34}S increases with assimilation of basalts altered by hydrothermal processes (comprising hydrothermal sulphides; Labidi et al., 2014). Fig. 8 shows that there is no co-variation between $\delta^{98/95}$Mo and δ^{34}S isotopes or Cl/K content of the glasses. In both cases, the most contaminated sample displays a composition similar to the range of variation observed in the uncontaminated domains. In fact, the largest $\delta^{98/95}$Mo variations are observed in the uncontaminated domains. This suggests that these two processes (magma interaction with hydrothermal brines and assimilation of hydrothermally altered crust) cannot account for the $\delta^{98/95}$Mo variations observed amongst Pacific–Antarctic MORBs, and are, therefore, also unlikely to affect magma compositions at other ridges.

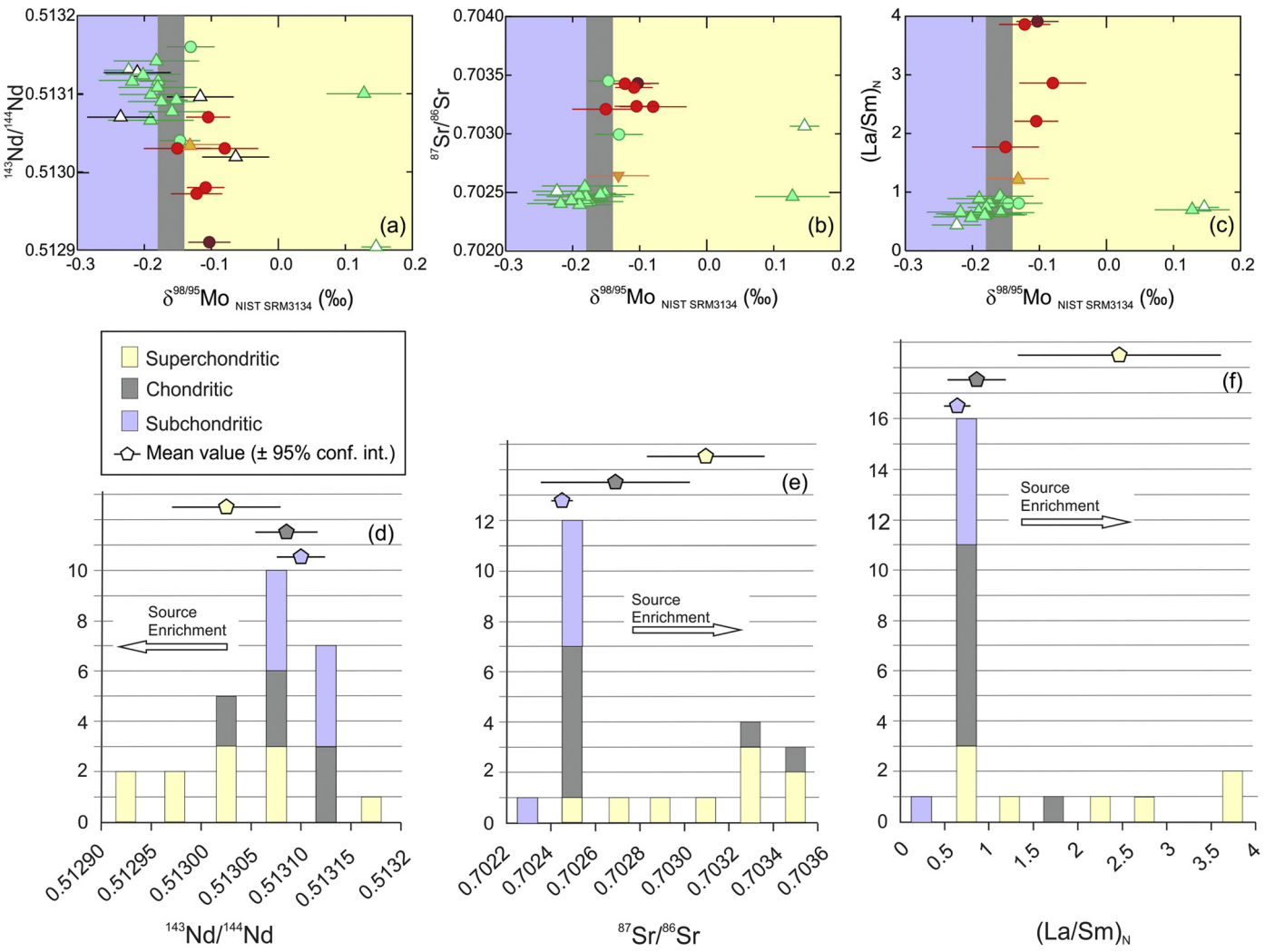

Fig. 6. $\delta^{98/95}$Mo variation with $^{143}Nd/^{144}Nd$, $^{87}Sr/^{86}Sr$ and $(La/Sm)_N$ for individual (a, b, c) and grouped (d, e, f) samples. In (d, e, f) samples are grouped based on their subchondritic, chondritic and superchondritic $\delta^{98/95}$Mo (Chondrite compositions of Burkhardt et al., 2014). Abbreviations in (a, b, c) as in Fig. 2.

4.3. Mantle partial melting

Mass-dependent isotopic fractionation during mantle partial melting has been documented to occur for some elements (e.g., Fe; Dauphas et al., 2009), but has yet to be investigated for Mo isotopes. Constraining the behaviour of Mo isotopes during partial melting is important to understand the extent to which all primitive magmas reflect their mantle source composition, but also to understand if the mantle composition was modified through time due to crust extraction.

The samples in this study were selected to cover a large range of partial melting degrees. Indeed, conceptually, magmas produced in the fast Pacific–Antarctic ridge should result from higher degrees of partial melting compared to those of the slow Mohns–Knipovich ridge (e.g. Klein and Langmuir, 1987). Furthermore, OIB lavas result from much lower degrees of partial melting than MORBs, hence magmas erupted at the Jan Mayen OIB should result from much lower degrees of melting than the MORBs at the Mohns–Knipovich ridge (e.g. Hofmann, 2003). However, finding a proxy to quantitatively constrain the degree of partial melting in mantle-derived magmas is not straightforward. Indeed, concentrations of incompatible elements such as Mo in mantle-derived magmas are largely influenced by the degree of melting but also by the source composition (e.g. Johnson et al., 1990). This is clearly illustrated by the correlation of Mo concentrations with $^{143}Nd/^{144}Nd$ shown in Fig. 7a. Thus, Mo concentrations cannot be used as a direct proxy for the degree of melting. Klein and Langmuir (1987) suggested that, except for a few cases, the $Na_{8.0}$ content of MORBs (the calculated Na_2O at MgO = 8 wt.%; see caption of Fig. 7 for equation), which can be calculated for samples with MgO between 5 and 8.5 wt.% (which is the case for 68% of the selected samples), was little impacted by source heterogeneities, making it the most suitable proxy to constrain the degree of partial melting. This is based on the global negative correlation between $Na_{8.0}$ and $Fe_{8.0}$ (FeO content at MgO = 8 wt.%; see caption of Fig. 7 for equation) observed for oceanic basalts; this trend is opposite to what would be expected if the $Na_{8.0}$ variations were produced by source fertility changes. Indeed, at similar degrees of melting, magmas produced by the melting of a more fertile source are expected to have both higher Na_2O and FeO contents than samples produced by the melting of a more depleted source. This would result in a positive, rather than negative correlation between $Na_{8.0}$ and $Fe_{8.0}$. A few exceptions exist, and the Jan Mayen hotspot region is one of them (Klein and Langmuir, 1987). As already highlighted by Klein and Langmuir (1987), source fertility variation is likely responsible for the offset between MORBs near Jan Mayen and other oceanic basalts. This is illustrated in our sample set by the displacement of the Mohns–Knipovich E-MORBs from the rest of the samples, shown in Fig. 7b. Therefore, only Mohns–Knipovich N-MORBs and the remaining Pacific–Antarctic samples hold po-

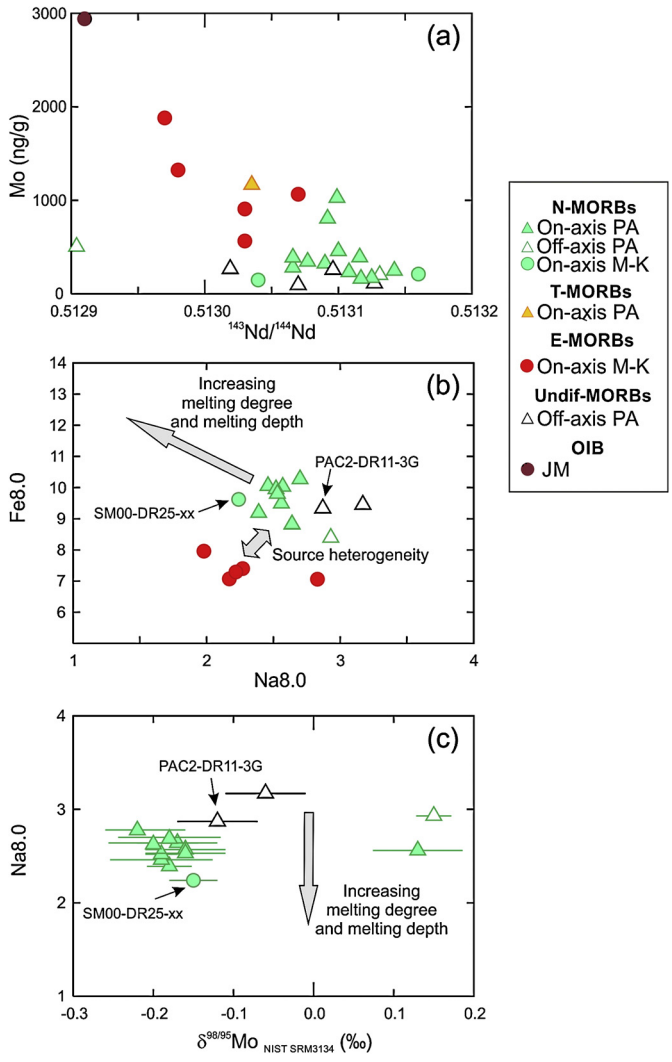

Fig. 7. (a) Mo (ng/g) vs. ^{143}Nd/^{144}Nd. (b) $Fe_{8.0}$ vs. $Na_{8.0}$ and (c) $Na_{8.0}$ vs. $\delta^{98/95}$Mo. $Na_{8.0}$ and $Fe_{8.0}$ are calculated for samples with MgO between 5 and 8.5 wt.% only, using Klein and Langmuir (1987) formulae: $Na_{8.0} = Na_2O + 0.373 * (MgO) - 2.98$; $Fe_{8.0} = FeO + 1.664 * (MgO) - 13.313$. All samples for which $Na_{8.0}$ and $Fe_{8.0}$ can be calculated are plotted in (b) while only samples relevant to estimate the effect of partial melting are presented in (c) (see section 4.3 for explanations). Abbreviations as in Fig. 2.

tential to assess the effect of partial melting on $\delta^{98/95}$Mo using $Na_{8.0}$. These samples form a flat to slightly negative correlation between $Na_{8.0}$ and $Fe_{8.0}$, consistent with a control by partial melting (Fig. 7b). Amongst these samples, those with contrasting $Na_{8.0}$, such as PAC2DR11-3G ($Na_{8.0}$ = 2.87) and SM00 DR25-xx ($Na_{8.0}$ = 2.24), show no $\delta^{98/95}$Mo disparity ($\delta^{98/95}Mo = -0.12 \pm 0.05$‰ versus -0.15 ± 0.03‰ respectively; Fig. 7b, c; Table 1). Since the difference in $Na_{8.0}$ between these two samples covers most of the range observed in the sample set, their similar $\delta^{98/95}$Mo suggests that the impact of partial melting on the $\delta^{98/95}$Mo of the magmas is negligible, at least at the scale of variations occurring amongst the investigated Pacific–Antarctic and Mohns–Knipovich N-MORBs. Furthermore, the ~0.6 difference in $Na_{8.0}$ between PAC2DR11-3G and SM00 DR25-xx represents ~30% of the global MORB-OIB $Na_{8.0}$ variations observed by Klein and Langmuir (1987), which corresponds to a ~3.5% difference in melting degree. Since oceanic basalts are suggested to be produced by ~8% to 20% of melting, this ~3.5% degree of melting would corresponds to between ~40 and ~17% of the absolute amount of melting involved in MORB production. Since no $\delta^{98/95}$Mo variation can be observed over this range, the impact of partial melting on the $\delta^{98/95}$Mo compositions of the magmas is likely limited during MORB production in general. Thus the Mo isotopic composition of MORBs likely represent those of their mantle sources. Nevertheless, to fully assess the effect of partial melting on magma $\delta^{98/95}$Mo compositions, it will be necessary to analyse samples covering the entire range of partial melting degrees relevant for MORB sources, ideally in conjunction with the analysis of mantle peridotites.

4.4. Mantle heterogeneities

4.4.1. $\delta^{98/95}$Mo and source enrichment

If the $\delta^{98/95}$Mo variations observed in the lavas are not produced during magma genesis and evolution, they are most likely caused by compositional variations in the mantle. As such, some correlations between $\delta^{98/95}$Mo and proxies of source depletion/enrichment such as REE ratios and radiogenic isotope compositions would be expected. Fig. 6a–c shows that relationships exist between $\delta^{98/95}$Mo and $(La/Sm)_N$, ^{87}Sr/^{86}Sr and ^{143}Nd/^{144}Nd (Fig. 6a, b, c), suggesting that mantle heterogeneities exert some control on Mo isotope variations. These links are better illustrated in Fig. 6c, d, e where the distribution of the samples, classified in subchondritic, chondritic and superchondritic $\delta^{98/95}$Mo compositions over the relevant ranges of ^{143}Nd/^{144}Nd, ^{87}Sr/^{86}Sr and $(La/Sm)_N$, are presented on stacked histograms. These figures show that samples with subchondritic $\delta^{98/95}$Mo only distribute over the most depleted ^{143}Nd/^{144}Nd, ^{87}Sr/^{86}Sr and $(La/Sm)_N$ compositions. In contrast, samples with chondritic $\delta^{98/95}$Mo dominantly distribute in the most enriched end of the subchondritic bins and, to a lower extent, in more enriched compositions. Finally, the superchondritic samples dominantly show more enriched compositions. Collectively these information show that, mantle sources with enriched ^{143}Nd/^{144}Nd, ^{87}Sr/^{86}Sr and $(La/Sm)_N$ compositions tend to have heavier $\delta^{98/95}$Mo.

However, it is also clear on the histograms that the spread of ^{143}Nd/^{144}Nd, ^{87}Sr/^{86}Sr and $(La/Sm)_N$ compositions also increase from the subchondritic to the superchondritic sample groups, precluding clear correlations between $\delta^{98/95}$Mo and these mantle enrichment proxies. In a context where $\delta^{98/95}$Mo variations in MORBs are controlled by source heterogeneities, an increasing dispersion of the data from subchondritic to superchondritic $\delta^{98/95}$Mo would not be surprising. Indeed, at least four other endmembers than the Depleted MORB Mantle (DMM) are involved in the sample sources (Hamelin et al., 2011; Blichert-Toft et al., 2005) and each of them is characterised by distinct radiogenic isotope compositions (as highlighted by the absence of a single mixing trend in the Sr–Nd and Nd–Pb isotope diagrams; Fig. 2). Based on the mixing lines, the Pacific–Antarctic MORBs likely all share a similar depleted endmember (the DMM; Hamelin et al., 2011) but the enriched endmember composition of the off-axis MORBs from the Menard TF differs from that of the rest of the samples (Fig. 2). Furthermore, the Mohns–Knipovich MORBs plot on a different mixing line than the Pacific–Antarctic MORBs (Fig. 2) suggesting that both of their source endmembers are different from those involved in the Pacific–Antarctic samples. All these mantle endmembers, with variably more enriched composition than the DMM are thought to be comprised of different crustal components and/or produced by different mantle processes (e.g., Hamelin et al., 2011; Blichert-Toft et al., 2005). As such, it seems likely that, in addition to showing different radiogenic isotopes and trace element ratios, these endmembers also have different $\delta^{98/95}$Mo at similar ^{143}Nd/^{144}Nd, ^{87}Sr/^{86}Sr and $(La/Sm)_N$. The variable origin and evolution of the mantle endmembers involved in the sample sources would also explain the absence of clear global relationships between $\delta^{98/95}$Mo and other isotopic systems, such as ^{176}Hf/^{177}Hf or $^{206/207/208}$Pb/^{204}Pb (see the Supplementary Material).

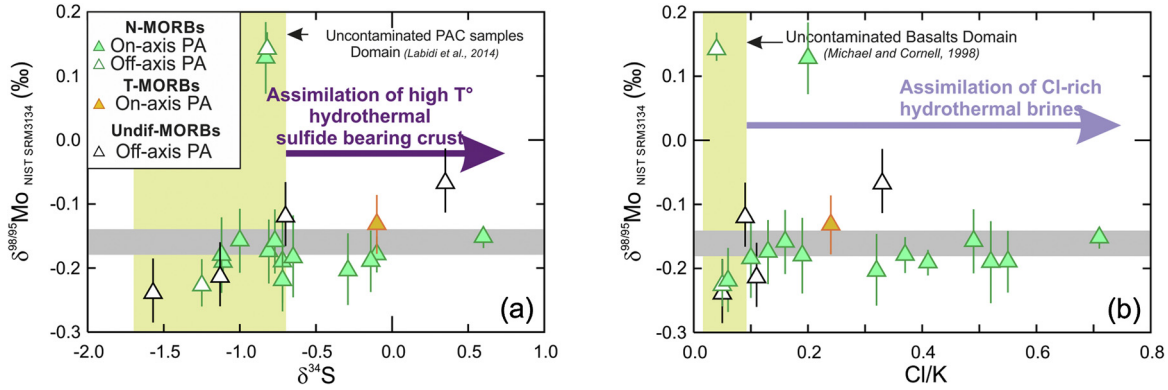

Fig. 8. Variation of $\delta^{98/95}$Mo with (a) δ^{34}S and (b) Cl/K. δ^{34}S and Cl/K values are from Labidi et al. (2014). Abbreviations as in Fig. 2. Grey field: chondrite compositions of Burkhardt et al. (2014).

In addition to the involvement of mantle endmembers with different $\delta^{98/95}$Mo, the limited correlations between $\delta^{98/95}$Mo and ^{143}Nd/^{144}Nd, ^{87}Sr/^{86}Sr and $(La/Sm)_N$ could in part result from the diluted amounts of enriched components in the MORB sources, resulting in an only limited spread in the data.

4.4.2. $\delta^{98/95}$Mo of the depleted mantle endmember

Pacific–Antarctic N-MORBs characterised by the most depleted composition best reflect the depleted mantle without any enrichment through addition of recycled crustal components (i.e., the DMM endmember; e.g., Hamelin et al., 2011). The results of the present study show that these samples display slightly subchondritic $\delta^{98/95}$Mo compositions. For instance, the five samples with the most radiogenic Nd isotope compositions (i.e., ^{143}Nd/^{144}Nd = 0.51317–0.51327) have a mean $\delta^{98/95}$Mo = -0.21 ± 0.02‰ (95% conf.), suggesting that the Mo stable isotope composition of the DMM is light compared to that of chondrites ($\delta^{98/95}$Mo = -0.16 ± 0.02‰; Burkhardt et al., 2014). Based on experimental work from Hin et al. (2013), the $\delta^{98/95}$Mo of the BSE can only be chondritic or heavier. Thus, the light Mo isotope composition of the DMM cannot reflect that of the BSE and, consequently, a mantle process needs to be involved to generate the lighter $\delta^{98/95}$Mo of the DMM compared to the BSE. There is only one process that is capable of modifying the $\delta^{98/95}$Mo of the mantle without enriching the source in terms of incompatible trace elements and radiogenic isotopes; this process is partial melting. This would require that previously extracted melts from the depleted mantle would have preferentially incorporated heavy Mo isotopes, leaving a residual mantle with lighter isotope signatures. Although we saw in section 4.3 that it is unlikely that partial melting involved in the production of MORBs themselves results in a significant departure of the $\delta^{98/95}$Mo of the magma from its source, this does not exclude that the composition of the mantle residue changes. As an incompatible element, Mo is strongly enriched in the melt over the residue, and so the effect of any isotopic fractionation during partial melting would be more pronounced in the mantle residue than in the MORBs themselves. Nevertheless, the isotopic fractionation produced by a single partial melting event may not be measurable and the sub-chondritic $\delta^{98/95}$Mo of the depleted MORB source is more likely the result of repeated magma extraction. In this case, the small isotopic fractionation imparted by each melting event would sum up to a measurable isotopic fractionation over time. Assuming that core equilibration did not fractionate Mo isotopes ($T > 2500$ °C), and the $\delta^{98/95}$Mo of the bulk Earth is chondritic, then partial melting would need to reduce the depleted mantle composition by 0.05 ± 0.04‰ to explain the most depleted Pacific–Antarctic MORBs (^{143}Nd/^{144}Nd = 0.51317–0.51327; $\delta^{98/95}$Mo = -0.21 ± 0.02‰). This would represent a minimum estimate, which would be increased if isotopic fractionation occurred during core formation.

4.5. Implication for the $\delta^{98/95}$Mo of the bulk silicate Earth

If magma extraction modified the $\delta^{98/95}$Mo composition of the DMM as suggested in section 4.4, then the $\delta^{98/95}$Mo of the BSE cannot directly be determined using MORBs, since the precise quantification of the impact of such process would be difficult. Thus, the analysis of lavas originating from other mantle reservoirs is necessary to fully assess the $\delta^{98/95}$Mo composition of the BSE. In this regard, the analysis of OIBs will be important, because these sample deeper and more primitive parts of the mantle. However, the effect of crust recycling on the $\delta^{98/95}$Mo composition of the mantle highlighted in section 4.4 will likely complicate the interpretation of the OIB data, because most OIB sources are thought to comprise recycled crustal components (e.g. White, 2015). Nevertheless, once the $\delta^{98/95}$Mo composition of the different OIB endmembers (e.g., HIMU, PREMA, EM I, EM II) are fully characterised, it might be possible to precisely constrain the $\delta^{98/95}$Mo of the BSE. Finally, some or all of the $\delta^{98/95}$Mo heterogeneities observed in the current mantle might already have existed during the Archean and, in this case, may be important for the interpretation of the $\delta^{98/95}$Mo signature of Archean komatiites previously used to determine the $\delta^{98/95}$Mo of the BSE (Greber et al., 2015).

5. Conclusions

Pacific–Antarctic and Mohns–Knipovich MORBs as well as the Jan Mayen OIB show variable $\delta^{98/95}$Mo ranging from -0.24‰ to $+0.15$‰. The absence of correlations between $\delta^{98/95}$Mo and indices of mineral fractionation, crust and hydrothermal brines assimilation as well as partial melting suggest that these processes have negligible impact on the Mo isotopic compositions of MORBs. Instead, $\delta^{98/95}$Mo tend to increase with indices of source enrichment such as ^{87}Sr/^{86}Sr, ^{143}Nd/^{144}Nd and $(La/Sm)_N$ suggesting mantle heterogeneities as the main driver for the variations observed. The DMM has a subchondritic $\delta^{98/95}$Mo that cannot be explained by core formation, and most likely is the result of repeated melt extraction from the mantle over geological timescales. The other, variably more enriched, mantle endmembers have heavier signatures than the DMM which suggest that the recycled crustal components involved are characterised by superchondritic $\delta^{98/95}$Mo compositions. Together, these observations imply that the $\delta^{98/95}$Mo composition of the BSE is unlikely to be preserved in the depleted mantle.

Acknowledgements

We are very grateful to Helen Ondreas, Joel Etoubleau, Sandrine Cheron and Manuel Moreira for providing several of the PAC1 and 2 samples. This research received funding to Thorsten Kleine from the European Research Council under the European Community's Seventh Framework Program (FP7/2007-2013 Grant Agreement 616564 'ISOCORE'). The constructive comments by three anonymous reviewers and the editorial handling by Bernard Marty are gratefully acknowledged.

Appendix A. Supplementary material

Supplementary material related to this article can be found online at http://dx.doi.org/10.1016/j.epsl.2016.07.056.

References

Blichert-Toft, J., Agranier, A., Andres, M., Kingsley, R., Schilling, J.-G., Albarède, F., 2005. Geochemical segmentation of the Mid-Atlantic Ridge north of Iceland and ridge-hot spot interaction in the North Atlantic. Geochem. Geophys. Geosyst. 6, Q01E19. http://dx.doi.org/10.1029/2004GC000788.

Brandl, P.A., Beir, C., Regelous, M., Abouchami, W., Haase, K.M., Garbe-Schonberg, D., Galer, S.J.G., 2012. Volcanism on the flanks of the East Pacific Rise: quantitative constraints on mantle heterogeneity and melting processes. Chem. Geol. 298–299, 41–56.

Burkhardt, C., Hin, R.C., Kleine, T., Bourdon, B., 2014. Evidence for Mo isotope fractionation in the solar nebula and during planetary differentiation. Earth Planet. Sci. Lett. 391, 201–211.

Cabral, R.A., et al., 2013. Anomalous sulphur isotopes in plume lavas reveal deep mantle storage of Archaean crust. Nature 496, 490–493.

Dauphas, N., Craddock, P.R., Asimow, P.D., Bennet, V.C., Nutman, A.P., Ohnenstetter, D., 2009. Iron isotopes may reveal the redox conditions of mantle melting from Archean to present. Earth Planet. Sci. Lett. 288, 255–267.

DeMets, C., Gordon, R., Argus, D., Stein, S., 1990. Current plate motions. Geophys. J. Int. 101, 425–478.

Dick, H.J.B., Lin, J., Schouten, H., 2003. An ultraslow-spreading class of ocean ridge. Nature 426, 405–412.

Dosso, L., Ondréas, H., Briais, A., Fernagu, P., Floch, G., Hamelin, C., Hannan, B.B., Klingelhoefer, F., Moreira, M., Normand, A., 2005. The Pacific–Antarctic Ridge between 41°150′S and 52°450′S: survey and sampling during the PACANTARCTIC 2 cruise. InterRidge News 14, 1–14.

Elkins, L.J., Hamelin, C., Blichert-Toft, J., Scott, S.R., Sims, K.W.W., Yeo, I.O., Devey, C.W., Pederson, R.B., 2016. North Atlantic hotspot–ridge interaction near Jan Mayen Island. Geochem. Perspect. Lett. 2, 55–67.

Freymuth, H., Vils, F., Willbold, M., Taylor, R.N., Elliott, T., 2015. Molybdenum mobility and isotopic fractionation during subduction. Earth Planet. Sci. Lett. 432, 176–186.

Georg, R.B., Halliday, A.N., Schauble, E.A., Reynolds, B.C., 2007. Silicon in the Earth's core. Nature 447, 1102–1106.

Goldberg, T., Gordon, G., Izon, G., Archer, C., Pearce, C.R., McManus, J., Anbar, A.D., Rehkämper, M., 2013. J. Anal. At. Spectrom. 28, 724–735.

Greber, N.D., Siebert, C., Nägler, T.F., Pettke, T., 2012. $\delta^{98/95}$Mo values and molybdenum concentration data for NIST SRM 610, 612 and 3134: toward a common protocol for reporting Mo data. Geostand. Geoanal. Res. 36, 291–300.

Greber, N.D., Pettke, T., Nägler, T.F., 2014. Magmatic–hydrothermal molybdenum isotope fractionation and its relevance to the igneous crustal signature. Lithos 190–191, 104–110.

Greber, N.D., Puchtel, I.S., Nägler, T.F., Mezger, K., 2015. Komatiites constrain molybdenum isotope composition of the Earth's mantle. Earth Planet. Sci. Lett. 421, 129–138.

Hamelin, C., Dosso, L., Hanan, B., Barrat, J-A., Ondreas, H., 2010. Sr–Nd–Hf isotopes along the Pacific Antarctic Ridge from 41 to 53°S. Geophys. Res. Lett. 37, L10303. http://dx.doi.org/10.1029/2010GL042979.

Hamelin, C., Dosso, L., Hanan, B.B., Moreira, M., Kositsky, A.P., Thomas, M.Y., 2011. Geochemical portray of the Pacific Ridge: new isotopic data and statistical techniques. Earth Planet. Sci. Lett. 302, 154–162.

Hin, R.C., Burkhardt, C., Schmidt, M.W., Bourdon, B., Kleine, T., 2013. Experimental evidence for Mo isotope fractionation between metal and silicate liquids. Earth Planet. Sci. Lett. 379, 38–48.

Hofmann, A.W., 2003. Sampling mantle heterogeneity through oceanic basalts: isotopes and trace elements. In: Carlson, R.W., Holland, H.D., Turekian, K.K. (Eds.), Treatise on Geochemistry, vol. 2. Elsevier, pp. 61–101.

Johnson, K.T.M., Dick, H.J.B., Shimizu , N., 1990. Melting in the oceanic upper mantle: an ion microprobe study of diopsides in abyssal peridotites. J. Geophys. Res. 95, 2661–2678.

Klein, E.M., Langmuir, C.H., 1987. Global correlations of ocean ridge basalt chemistry with axial depth and crustal thickness. J. Geophys. Res. 92, 8089–8115.

König, S., Wille, M., Voegelin, A., Schoenberg, R., 2016. Molybdenum isotope systematics in subduction zones. Earth Planet. Sci. Lett. 447, 95–102.

Labidi, J., Cartigny, P., Hamelin, C., Moreira, M., Dosso, L., 2014. Sulfur isotope budget (32S, 33S, 34S and 36S) in Pacific–Antarctic ridge basalts: a record of mantle source heterogeneity and hydrothermal sulfide assimilation. Geochim. Cosmochim. Acta 133, 47–67.

Michael, P., Cornell, W., 1998. Influence of spreading rate and magma supply on crystallization and assimilation beneath mid-ocean ridges: evidence from chlorine and major element chemistry of mid-ocean ridge basalts. J. Geophys. Res. 103, 18325-18.

Moreira, M., Dosso, L., Ondréas, H., 2008. Helium isotopes on the Pacific–Antarctic ridge (52.5–41.5°S). Geophys. Res. Lett. 35, 1–6.

Neubert, N., Heri, A.R., Voegelin, A.R., Nägler, T.F., Schlunegger, F., Villa, I.M., 2011. The molybdenum isotopic composition in river water: constraints from small catchments. Earth Planet. Sci. Lett. 304, 180–190.

Rubin, K., Sinton, J., Mclennan, J., Hellebrand, E., 2009. Magmatic filtering of mantle compositions at mid-ocean-ridge volcanoes. Nat. Geosci. 2, 321–328.

Rudge, J.F., Reynolds, B.C., Bourdon, B., 2009. The double spike toolbox. Chem. Geol. 265, 420–431.

Siebert, C., Nägler, T.F., von Blanckenburg, F., Kramers, J.D., 2003. Molybdenum isotope records as a potential new proxy for paleoceanography. Earth Planet. Sci. Lett. 211, 159–171.

Vlastélic, I., Aslanian, D., Dosso, L., Bougault, H., Olivet, J.L., Géli, L., 1999. Large-scale chemical and thermal division of the Pacific mantle. Nature 399, 345–350.

Vlastélic, I., Dosso, L., Bougault, H., Aslanian, D., Géli, L., Etoubleau, J., Bohn, M., Joron, J.L., Bollinger, C., 2000. Chemical systematics of an intermediate spreading ridge: the Pacific–Antarctic Ridge between 56°S and 66°S. J. Geophys. Res. 105, 2915–2936.

Voegelin, A.R., Nägler, T.F., Pettke, T., Neubert, N., Steinmann, M., Pourret, O., Villa, I.M., 2012. The impact of igneous bedrock weathering on the Mo isotopic composition of stream waters: natural samples and laboratory experiments. Geochim. Cosmochim. Acta 86, 150–165.

Voegelin, A.R., Pettke, T., Greber, N.D., von Niederhäusern, B., Nägler, T.F., 2014. Magma differentiation fractionates Mo isotope ratios: evidence from the Kos Plateau Tuff (Aegean Arc). Lithos 190–191, 440–448.

Weis, D., Kieffer, B., Maerschalk, C., Pretorius, W., Barling, J., 2005. High-precision Pb–Sr–Nd–Hf isotopic characterization of USGS BHVO-1 and BHVO-2 reference materials. Geochem. Geophys. Geosyst. 6 (2). http://dx.doi.org/10.1029/2004GC000852.

White, W.M., 2015. Isotopes, DUPAL, LLSVPs and Anekantavada. Chem. Geol. 419, 10–28.

Willbold, M., Hibbert, K., Lai, Y.-J., Freymuth, H., Hin, R.C., Coath, C., Vils, F., Elliott, T., 2016. High-precision mass dependent molybdenum isotope variations in magmatic rocks determined by double-spike MC-ICP-MS. Geostand. Geoanal. Res. http://dx.doi.org/10.1111/j.1751-908X.2015.00388.x.

Yang, J., Siebert, C., Barling, J., Savage, P., Liang, Y.-H., 2015. Absence of molybdenum isotope fractionation during magmatic differentiation at Hekla volcano, Iceland. Geochim. Cosmochim. Acta 162, 126–136.